Nuclear Instruments and Methods in Physics Research B 310 (2013) 93–98

Contents lists available at SciVerse ScienceDirect

Nuclear Instruments and Methods in Physics Research B

journal homepage: www.elsevier.com/locate/nimb

Structural and mechanical properties of magnetron sputtered Ti–V–Cr–Al–N films

Du-Cheng Tsai [a], Zue-Chin Chang [b], Bing-Hau Kuo [a], Ming-Hua Shiao [c], Fuh-Sheng Shieu [a,*]

[a] Department of Materials Science and Engineering, National Chung Hsing University, Taichung 40227, Taiwan
[b] Department of Mechanical Engineering, National Chin-Yi University of Technology, Taichung 41170, Taiwan
[c] Instrument Technology Research Center, National Applied Research Laboratories, Hsinchu 300, Taiwan

ARTICLE INFO

Article history:
Received 13 March 2013
Received in revised form 11 April 2013
Available online 19 April 2013

Keywords:
Coating materials
Nitride materials
Thin films
Vapor deposition
Crystal structure

ABSTRACT

Ti–V–Cr–Al–N films were prepared by dc magnetron co-sputtering by utilizing TiVCr and Al targets. By using glancing incidence X-ray diffraction, a single NaCl solid solution phase with (200) preferred orientation for the Al-doped films was revealed, as opposed to the undoped films that possessed predominantly (111) preferred orientation. This indicates that Al addition can lead to the enhancement of adatom mobility and consequently, to a thermodynamically favorable (200) orientation. This also leads to grain growth and increased surface roughness. However, based on results from transmission electron microscopy, the microstructure morphology seemed independent of the Al concentration, implying that adatom mobility is not sufficient for the barriers present at the grain boundaries. Accordingly, hardness was enhanced by the increase in Al concentration.

© 2013 Elsevier B.V. All rights reserved.

1. Introduction

Binary transition metal nitride films, such as TiN and CrN, among others, are widely used to increase the application range of underlying materials. Increasing the hardness of the films, as well as ensuring their appropriate chemical and thermodynamical stability, can protect materials from damage in aggressive environments [1–4]. To improve these properties, the best known method is adding a third element such as Al and Si to form solid solution and nanocomposite films. Several recent studies have shown that ternary nitride films in Ti–Al–N, Cr–Al–N, Ti–Si–N, and Cr–Si–N systems have improved hardness and thermal stability, which provide significant improvements in various applications [5–8]. Moreover, great efforts have also been done by alloying nitride film with other elements, such as Ti–Cr–N, Cr–V–N, and Ti–V–N [9–11]. They exhibited improved mechanical properties and thermal stability. In view of the foregoing, depositing multi-element mixed films would be an effective path to developing further the properties of material.

More recently, Ti–V–Cr–N films with three strong nitride forming elements were designed to deposit strong nitride films by dc magnetron reactive sputtering [12]. The crystal structures, microstructure, and mechanical and electrical properties were investigated in detail. The influence of Al contents in binary nitrides is intensively investigated in literature, but the role of Al content in Ti–V–Cr–N films is not yet clarified. This study is thus intended to investigate the Al effect on Ti–V–Cr–N films by dc magnetron reactive co-sputtering of equi-molar TiVCr and Al targets. The Al input powers is monitored to prepare different Al-containing coatings for investigating the Al effect on the structure, mechanical and electrical properties.

2. Experimental

Ti–V–Cr–Al–N films were formed in an high-vacuum dual-target sputter deposition system by dc magnetron sputtering onto the p-type Si(100) substrate using 4-inch-diameter TiVCr and Al targets in a pure N_2 atmosphere (Fig. 1). Prior deposition, p-Si (100) wafers were cleaned in an ultrasonic bath and then rinsed thoroughly with ethanol and distilled water, after which they were placed in the vacuum system. In carrying out dual-target sputter deposition, the distance of the target to the substrate was 150 mm and the deposition angle was 45° relative to the substrate. The sputtering system consisted of a stainless steel vacuum chamber and a cryopump with a rotary pump, providing an ultimate vacuum of 6.67×10^{-5} Pa before introducing the gases. High-purity nitrogen (4 N) was used as sputtering gas. Nitrogen flow was kept at 70.5 standard cubic centimeters per minute (sccm). TiVCr target power was 300 W with Al target power ranging from 0 to 300 W in order to obtain $(TiVCr)_{1-x}Al_x$ nitride films with a different content of Al. During deposition, the working pressure was kept at 4.0×10^{-1} Pa and the deposition time was

* Corresponding author. Address: Department of Materials Science and Engineering, National Chung Hsing University, Taichung 40227, Taiwan. Tel.: +886 4 2284 0500; fax: +886 4 2285 7017.
E-mail address: fsshieu@dragon.nchu.edu.tw (F.-S. Shieu).

0168-583X/$ - see front matter © 2013 Elsevier B.V. All rights reserved.
http://dx.doi.org/10.1016/j.nimb.2013.04.033

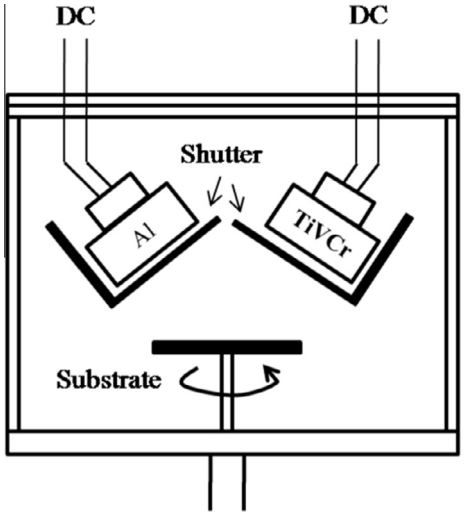

Fig. 1. Schematic diagram of the reactive magnetron sputtering system.

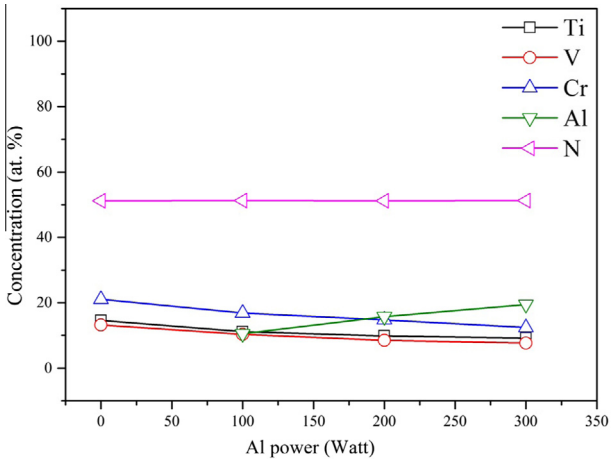

Fig. 2. ESCA determined composition of the Ti–V–Cr–Al–N thin films prepared at various input power of Al target.

set to 100 min. The substrates were rotated at 30 rpm during deposition in order to produce smooth and uniform films. The process parameters are listed in Table 1. The TiVCr and Al targets were presputtered in pure argon atmosphere to remove the surface oxide layer of the target before deposition.

The chemical compositions of the nitride films were analyzed by electron spectroscopy for chemical analysis (ESCA, PHI 500 VersaProbe). Crystalline structures were analyzed by glancing-incidence (1°) X-ray diffractometer (XRD, MacScience MXP3) using Cu Kα radiation at a scanning speed of 0.2°/min. Furthermore, based on the full width at half maximum, the average grain sizes of the films were calculated using Scherrer's formula [13]. Morphology studies and thickness measurements were carried out using field emission scanning electron microscopy (SEM, JEOL JSM-6700F). Microstructural examinations were conducted with an analytical transmission electron microscope (TEM, JEM 1200EX II). The surface morphology of the films was observed by atomic force microscopy (AFM, Seiko SPA400). The root mean square (RMS) surface roughness values of the films were derived from the AFM images. The microhardness and elastic modulus of the films were measured at a load of 200 μN using a TriboLab nanoindenter (Hysitron).

3. Results and discussion

Fig. 2 presents the ESCA-determined composition of the Ti–V–Cr–Al–N thin films prepared at various input powers of the Al target. By varying the power on the Al target, the chemical composition of thin films was controlled separately. The N concentration did not significantly vary with Al concentration, maintaining almost constant at values of 50 at.%; hence, this can be regarded as saturated nitride films.

Table 1
Deposition conditions of the Ti–V–Cr–Al–N films.

Process parameter	Values
Base pressure (Pa)	$<6.67 \times 10^{-5}$
Working pressure (Pa)	4.0×10^{-1}
N_2 flow (sccm)	70.5
Dc power on the TiVCr target (W)	300
Dc power on the Al target (W)	0, 100, 200, 300
Deposition time (min)	100
Deposition temperature	Room temperature
Target-to-substrate distance (mm)	150

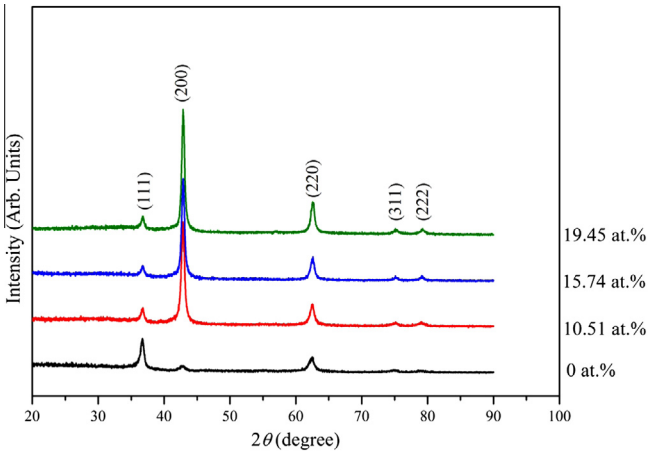

Fig. 3. X-ray diffraction pattern of the Ti–V–Cr–Al–N thin films with various Al concentrations.

Table 2
Relative intensities of diffraction peaks and average grain sizes of the Ti–V–Cr–Al–N films.

Al concentration (at.%)	Relative intensity			XRD-measured average grain size (nm)
	(111)	(200)	(220)	
0	62.4	9.4	28.3	11.9
10.51	25.8	206.0	43.9	14.4
15.74	19.5	210.7	44.9	15.6
19.45	23.2	254.4	66.8	16.0

Fig. 3 shows X-ray diffraction pattern of the Ti–V–Cr–Al–N thin films with various Al concentrations. Results indicate that all of the films exhibited a single NaCl solid solution structure. This is possible because TiN, VN, and CrN were all present in the NaCl structure. (TiVCr)N thin films also exhibited a single NaCl solid solution structure. Although AlN exhibited a wurtzite structure with alternating layers of Al and N atoms when approaching thermodynamically favorable situations, it also presented an NaCl metastable structure under high-pressure conditions. Typically, another method of obtaining the NaCl phase is epitaxial stabilization. Metastable structures can be stabilized by multilayer superlattices. Therefore,

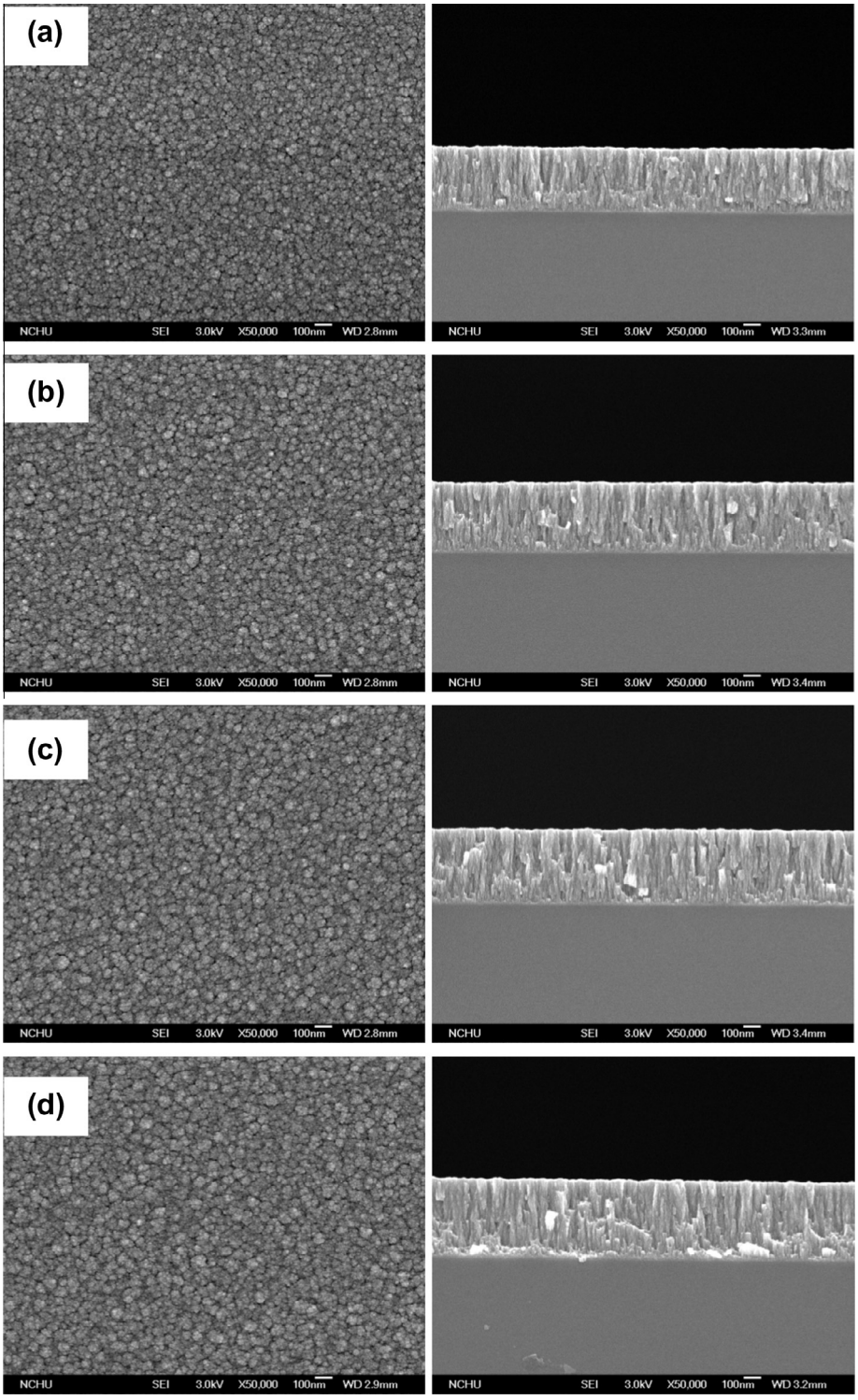

Fig. 4. Plan-view and cross-sectional SEM micrographs for the Ti–V–Cr–Al–N thin films with various Al concentrations. (a) 0 at.%, (b) 10.51 at.%, (c) 15.74 at.%, and (d) 19.45 at.%.

(TiVCrAl)N thin films can also exhibit a single NaCl solid solution structure in which Al, Ti, V, and Cr atoms are randomly distributed over the metal sublattice. The relative theoretically predicted and experimental results have already been reported by many studies. A single NaCl structure was exhibited in Ti–Al–N, Cr–Al–N, Ti–Cr–N, Cr–V–N, and Ti–V–N systems [5,6,9–11]. Additionally, Kimura et al. systematically showed that (TiAl)N and (CrAl)N films presented a single NaCl structure even if the Al ratio is increased to about 0.6 [14,15]. (TiCrAl)N films can also be synthesized with B1 structures up to an Al ratio of 0.73 [16]. The solubility limits of AlN incorporated into several transition nitrides with NaCl structure has been predicted by Makino [17] using the structural map constructed from two band parameters; the critical concentrations of AlN in TiN, VN, and CrN for phase change are 65.3%, 72.4%, and 77.2%, respectively. All the investigations mentioned above completely concur with our results.

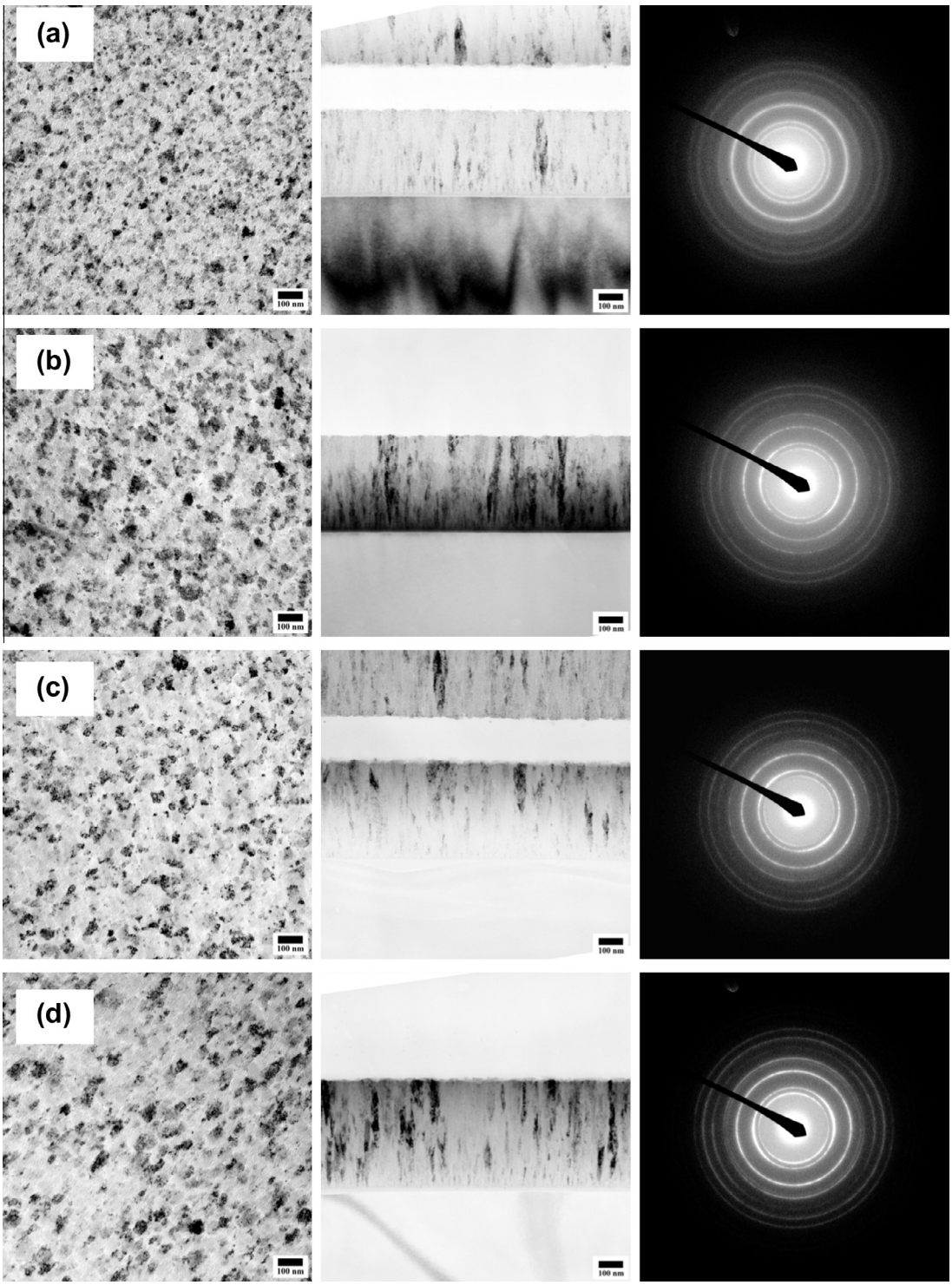

Fig. 5. Plan-view, cross-sectional TEM micrographs, and selected area diffraction patterns of the Ti–V–Cr–Al–N thin films with various Al concentrations. (a) 0 at.%, (b) 10.51 at.%, (c) 15.74 at.%, and (d) 19.45 at.%.

(TiVCr)N films exhibited a predominantly (111) preferred orientation with minor crystallites oriented at (200), (220), (311), and (222). However, this predominant preferential orientation in (TiVCrAl)N films transformed into a (200) preferred orientation. Moreover, the crystalline and grain size of the (TiVCrAl)N films significant increased with increase in Al concentration. The relative intensities of the diffraction peaks are listed in Table 2. Interestingly, the structure observed for the Ti–V–Cr–Al–N thin films were significantly modified by the addition of Al atoms. This indicates that the substitution of TiVCr atoms by Al in the metallic sublattice leads to a significant enhancement of adatom mobility on the growing crystallite. According to several authors [18–20], the transition from (111) to (200) of the predominant preferential orientation can also occur in TiN, CrN, and ZrN films after adding Al atoms. Therefore, the different activation energies of Ti in TiN and of Al in TiN play important roles. A wide range of activation

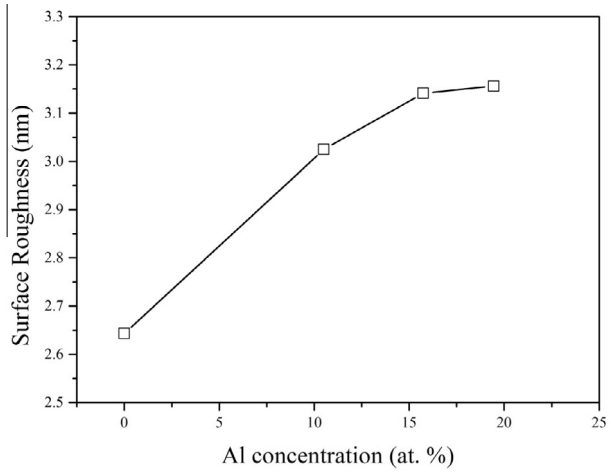

Fig. 6. Surface roughness of the Ti–V–Cr–Al–N thin films with various Al concentrations.

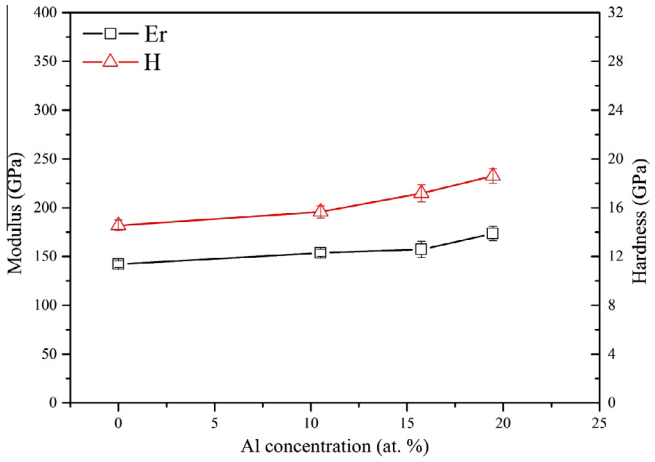

Fig. 7. Hardness of the Ti–V–Cr–Al–N thin films with various Al concentrations.

energies for atomic diffusion in TiN (2.1–2.2 eV for N and 2.6 eV for Ti) was reported previously [21]; for Al atoms, the activation energy of 0.3 eV was mentioned for Al diffusion along the grain boundaries in TiN. As the diffusion activation energy of Al is much lower than that of Ti in TiN, the diffusivity of atoms is enhanced. In other words, the substitution of Ti, V, and Cr atoms by Al atoms in the metallic sublattice leads to a significant enhancement of adatom mobility on growing films and consequently, to a thermodynamically favorable (200) orientation.

Fig. 4 shows the plan view and cross-sectional SEM micrographs of the Ti–V–Cr–Al–N thin films with various Al concentrations. One can notice a typical columnar structure with a dome-like surface. The individual columns, however, are compact and hard to separate. Evidently, even if the Al concentration was increased to 19.45 at.%, no significant changes in the morphology of undoped and Al-doped state could be observed.

Fig. 5 shows the plan view, cross-sectional TEM micrographs, and selected area diffraction (SAD) patterns of Ti–V–Cr–Al–N thin films with various Al concentrations. On top of the Si substrate, there is a randomly oriented small grain Ti–V–Cr–Al–N layer and a columnar Ti–V–Cr–Al–N layer. It is believed that in the initial stage of deposition, Ti–V–Cr–Al–N films nucleate to form randomly oriented small grains, leading to reduced surface energy; thereafter, they develop into grains (column) with larger lateral sizes along the growing direction, after which they produce typical V-shaped columns that are typical for transition (T zone) morphology [22]. The overall microstructure was quite compact, but void boundaries were still visible. When Al atoms were introduced into films from 0 at.% to 19.45 at.%, the microstructure did not exhibit any significant variation. This implies that the addition of Al can only cause significant increases in surface diffusion along the planes; however, an increase in adatom mobility proves insufficient to overcome the barrier located at the boundary. In effect, the microstructures of the thin films were all similar. Similar to XRD result, SAD patterns analysis shows that the films only exhibit a simple NaCl solid solution structure.

Fig. 6 shows the RMS surface roughness of the Ti–V–Cr–Al–N thin films as a function of Al concentration. With increase in Al concentrations, surface roughness also increased, but only very slightly. This variation in surface roughness conforms to that of grain size. This could be attributed to the enhanced adatom mobility causing grain aggregation or growth, thereby promoting the development of surface roughness.

Fig. 7 shows the hardness of Ti–V–Cr–Al–N thin films as a function of Al concentration. Pure (TiVCr)N film exhibited hardness of 14.6 GPa. Hardness and elastic modulus intensified with increase in Al concentration (i.e., up to 18.6 GPa and 173.6 GPa for an Al concentration of 19.45 at.%, respectively.). The hardening of the Ti–V–Cr–Al–N films as a function of the Al concentration could be attributed to solid solution strengthening and the hindered dislocation motion caused by lattice distortion. In addition, valence electron concentrations could have also affected the bonding state. Specifically, reduced valence electrons, which were contributed by the Al atom, decreased the retention of the anti-bonding states, thereby partially strengthening the stability and hardness of the structure [23]. In this study, chemical mixing enthalpy assisted the authors in investigating the phenomenon. The chemical mixing enthalpy of Al–Ti, Al–V, and Al–Cr were −30, −16, and −10 kJ mol^{-1}, respectively; meanwhile, the chemical mixing enthalpy of Ti–V, Ti–Cr, and V–Cr were −2, −7, and −2 kJ mol^{-1}, respectively [24]. Results imply that the combinative force of Al with other elements was strongest among all the elements in the alloy. As reported by Chung et al. [25], hardness intensifies with increase in Al concentration.

4. Conclusions

The influence of Al incorporation into (TiVCr)N in terms of microstructure and morphology, as well as electronic and mechanical properties, was studied using films deposited by a dual dc magnetron co-sputtering system onto TiVCr and Al targets. Pure (TiVCr)N films exhibited predominantly (111) preferred orientation, with minor amounts of crystallites preferentially oriented at (220), (311), and (222). When Ti, V, and Cr were substituted with Al, the aforementioned preferential orientation predominantly transformed into a (200) preferred orientation; grain growth was also promoted. Results indicate that adatom mobility can be enhanced by adding Al. Such findings can be attributed to lower diffusion activation energy of Al in TiN. Surface roughness was affected by grain growth. Accordingly, hardness intensified with increase in Al concentration, which could be attributed to solid solution strengthening and strong covalent bonds.

References

[1] T.S. Yeh, J.M. Wu, L.J. Hu, Thin Solid Films 516 (2008) 7294–7298.
[2] M.H. Shiao, Z.C. Chang, F.S. Shieu, J. Electrochem. Soc. 150 (2003) C320–C324.
[3] H. Liu, Q. Xu, X. Zhang, C. Wang, B. Tang, Nucl. Instrum. Methods Phys. Res., Sect. B 297 (2013) 1–6.
[4] W. Ensinger, S. Flege, M. Kiuchi, K. Honjo, Nucl. Instrum. Methods Phys. Res., Sect. B 272 (2012) 437–440.
[5] H.C. Barshilia, K. Yogesh, K.S. Rajam, Vacuum 83 (2008) 427–434.

[6] B. Tlili, N. Mustapha, C. Nouveau, Y. Benlatreche, G. Guillemot, M. Lambertin, Vacuum 84 (2010) 1067–1074.
[7] G. Zhang, L. Wang, S.C. Wang, P. Yan, Q. Xue, Appl. Surf. Sci. 255 (2009) 4425–4429.
[8] C.L. Chang, C.T. Lin, P.C. Tsai, W.Y. Ho, D.Y. Wang, Thin Solid Films 516 (2008) 5324–5329.
[9] J. Vetter, H.J. Scholl, O. Knotek, Surf. Coat. Technol. 74–75 (1995) 286–291.
[10] M. Uchida, N. Nihira, A. Mitsuo, K. Toyoda, K. Kubota, T. Aizawa, Surf. Coat. Technol. 177–178 (2004) 627–630.
[11] H. Hasegawa, A. Kimura, T. Suzuki, J. Vac. Sci. Technol. A 18 (2000) 1038–1040.
[12] D.C. Tsai, Y.L. huang, S.R. Lin, D.R. Jung, F.S. Shieu, Nucl. Instrum. Methods Phys. Res., Sect. B 269 (2011) 685–691.
[13] H.P. Klug, L.E. Alexander, X-ray Diffraction Procedures for Polycrystalline, Amorphous Materials, Wiley, New York, 1974.
[14] M. Zhou, Y. Makino, M. Nose, K. Nogi, Thin Solid Films 339 (1999) 203–208.
[15] A. Kimura, M. Kawate, H. Hasegawa, T. Suzuki, Surf. Coat. Technol. 169–170 (2003) 367–370.
[16] K. Yamamoto, T. Sato, K. Takahara, K. Hanaguri, Surf. Coat. Technol. 174–175 (2003) 620–626.
[17] Y. Makinoa, Surf. Coat. Technol. 193 (2005) 185–191.
[18] A. Kimura, H. Hasegawa, K. Yamada, T. Suzuki, Surf. Coat. Technol. 120–121 (1999) 438–441.
[19] M. Kawate, A. Kimura, T. Suzuki, J. Vac. Sci. Technol. A 20 (2002) 569–571.
[20] H. Hasegawa, M. Kawate, T. Suzuki, Surf. Coat. Technol. 200 (2005) 2409–2413.
[21] L. Hultman, Vacuum 57 (2000) 1–30.
[22] R. Messier, A.P. Giri, R.A. Roy, J. Vac. Sci. Technol. A 2 (1984) 500–503.
[23] C. Wang, P. Han, L. Zhang, C. Zhang, X. Yan, B. Xu, J. Alloy Compd. 482 (2009) 540–543.
[24] F.R. de Boer, R. Boom, W.C.M. Mattens, A.R. Miedema, A.K. Niessen, Cohesion in Metals, North-Holland, Amsterdam, 1988.
[25] C.K. Chung, T.S. Chen, J. Electrochem. Soc. 156 (2009) H119–H122.